doi: 10.56761/EFRE2022.N4-O-037802

Properties of ultrananocrystalline diamond grown under different deposition conditions

A. Gaydaychuk[*], *S. Linnik*, *A. Mitulinsky*, *S. Zenkin*

National Research Tomsk Polytechnic University, Tomsk, Russia
[*]*Gaydaychuk@tpu.ru*

Abstract. The influence of CH_4 and N_2 concentration in $CH_4/H_2/N_2$ gas mixture on microstructure and mechanical properties of diamond films is investigated. Nitrogen addition to the gas mixture up to 18.5 vol. % does not significantly affect the structure of the coating. In the entire range of gas concentrations, coating structure is represented by a set of dendrites consisting of diamond crystallites of various sizes, as well as non-diamond carbon. It is shown that CH_4 has a greater effect on the coating hardness and Young's modulus. Besides, it has been found that nitrogen-doped diamond coatings have a higher level of tensile residual stress. With a decrease in coating thickness or nitrogen concentration in the gas mixture, this difference decreases.
Keywords: diamond film; HFCVD; microstructure; nitrogen-doped films.

1. Introduction

Nanocrystalline diamond film (NCD film) is material with outstanding properties, widely used in various field of science and technology. Thus, NCD films are used: as cutting tools protective coatings for highly abrasive and composite materials machining [1, 2], protective coatings for multiphase pumps mechanical seals [3] and as a class of materials for biomedical field [4], optics [5] and electronics [6].

Due to the fact, that H_2/CH_4 gas mixture is the most commonly used for diamond film hot filament (HF) or microwave plasma assisted (MW) chemical vapor deposition (CVD), the first method for NCD film deposition is increased content of methane in the working gas mixture. Generally, CH_4 concentration varies from 3 to 10 vol. % [7, 8]. The second most common way to NCD film deposition is small nitrogen addition to the working gas mixture. According to scientific reports, nitrogen can both improve the quality and deposition rate of the diamond coating and be the reason for the micro- to nanocrystalline structure transition [9–12].

As stated above diamond film is the attractive material for cutting tools protective costings, especially for machining of composite materials such as carbon fiber reinforced plastics (CFRP) and etc. Despite the knowledge, the diamond-hard alloy system adhesive strength is still remain the main issue. Besides, high demands on the quality of machined surface require fine tuning of the film properties, such as the level of residual stress, coating architecture and surface roughness.

It should be noted that the most of reports are focused on the study of electrical properties of N-doped diamond films [13–16]. Nevertheless, there are separate works dedicated to improving the performance of diamond-coated cutting tools due to their doping with nitrogen [17–19].

Another issue that receives sufficient attention is the evolution of diamond film microstructure with varying of working gas mixture composition [20–23]. According to [20, 23] even a small addition of nitrogen to the CH_4/H_2 gas mixture leads to a significant change in the microcrystalline structure of the diamond coating. With the addition of 0.9 vol. % N_2, the coating structure consists of large diamond crystallites and ultra-small diamond clusters. Increase in N_2 content to 7 vol. % leads to diamond crystallites agglomeration into large elongated aggregates with a size of several hundreds of nanometers. In another report [21], diamond coating was synthesized using a $H_2/CH_4/B(CH_3)_3$ gas mixture with a methane (CH_2:H_2) content of 5–10% and boron (B:C) of 3000 ppm. As a result, deposited coating had a structure, as named, "nano feather" with a shaft up to a micron long and a lateral size in the range of 10–50 nm.

Despite the diamond films properties well studied, some aspects still remain fragmentary, and a fairly large part of the presented data with significant disagreement. In this regard, the aim of this

work is to study the effect of methane and nitrogen concentrations on the structure and properties of the diamond coating.

2. Materials and experimental methods

The mirror-polished Si (1 0 0) wafer of dimension 5×20×0.38 and 10×20×4 mm were used as substrates. As a pretreatment procedure, all types of substrates were consistently ultrasonicated in acetone, aqueous solution of nano-diamond (5–9 nm) and again in acetone. This step is necessary to clean the substrate and increase the nucleation density of diamond crystallites.

The diamond films deposition was carried out in a self-made HFCVD supply. Working gases (H_2, CH_4, N_2) were adjusted by mass flow controllers. The compositions of the working gas mixture, as well as the concentration of individual gases, are presented in Table 1. The value of CH_4 concentration in N_2 doped NCD films deposition experiment was chosen based on the threshold value for the microcrystalline diamond film synthesis. The minimum value of the nitrogen concentration in the gas mixture was selected experimentally by gradually increasing its content from 0.5 vol. % and higher. Temperature of the samples throughout all experiments was maintained at 850±20°C. The filament-substrate distance was 10±1 mm. The operating pressure was maintained at 20±2 Torr throughout the synthesis using a needle valve. In order to obtain accurate data, four samples of each type of coatings were studied in the experiments.

Table 1. Working gas mixture composition

	Gas flow, ml/min		
	CH_4	**H_2**	**N_2**
N1.n	14	100	
N2.n	19		0
N2.n	24		
NN1.n			8
NN2.n	6		16
NN3.n			24

n – rated diamond film thikness (4, 7, 10)

Phase purity of the diamond films was evaluated by X-ray diffraction analysis in glancing incidence mode (5°) using Cu-Kα ($\lambda = 0.154$ nm) radiation (Shimadzu XRD 6000). The surface morphology and films structure were analyzed by SEM (JSM-7500F, JEOL), AFM (NTGRA, NT-MDT), TEM (JEM-2100F, JEOL) and 3D optical profilometer (MICRO MEASURE 3D station, STILL). Raman spectra were recorded using a NanoScan Technology Centaur IHR spectrometer with 514.5 nm argon ion laser. The Nanoindenter G200 (MTS-Agilent) was used to determine the nanohardness of diamond coatings. The 30 mN indentation load was constant for all samples. A series of 10 indentations was made for each sample.

3. Results and discussions

Fig.1 shows the XRD and Raman spectra of the diamond films synthesized under different N_2/C ratios. As can be seen in Fig.1a and 1b, all spectra exhibit typical pattern of polycrystalline diamond with diffraction peaks at $2\Theta \sim 44°$, 75.4° and 91.6°, which correspond to the (1 1 1), (2 2 0) and (3 1 1) reflections of the diamond, respectively. All films have tensile residual stress, which follows from the shift of peaks position towards higher diffraction angles from the tabular values ($2\Theta = 41°$). (1 1 1) is the basic orientation for all films. For N-series, with an increase in CH_4 concentration, the diamond reflex intensities ratio ($I_{(220)}/I_{(111)}$ and $I_{(311)}/I_{(111)}$) decreases from 0.12 and 0.18 for N1.4 to 0.006 and 0.007 for N3.4, respectively. For NN-series, with an increase in N_2 concentration, intensities ratio ($I_{(220)}/I_{(111)}$ and $I_{(311)}/I_{(111)}$) decreases from 0.25 and 0.08 for NN1.4

to 0.19 and 0.07 for NN3.4, respectively. It is obvious that approximately threefold change in the nitrogen concentration in the gas mixture (from 7 to 18.5 vol. %) does not have a significant effect on the diamond crystallites orientation. Since diffraction peaks broadening is caused by an increase in the number of grain boundaries (a decrease in the size of diamond crystallites) its parameter was also analyzed. Thus, with a twofold increase in CH_4 concentration, the FWHM value for (1 1 1) peak increased from 1.35 to 2.6°. In the case of a similar increase in the nitrogen concentration, the FWHM value changed from 1.33 to 2.04°. The decrease in the size of diamond crystallites was also confirmed by calculation of coherent scattering region values (CSR) for presented series of samples according to the Scherer equation [24]. Thus, for samples N1.4, N2.4, and N3.4, the CSR values were 6.6, 4, and 3.4 nm, and for samples NN1.4, NN2.4, and NN3.4 – 6.7, 5.9, and 4.3 nm, respectively.

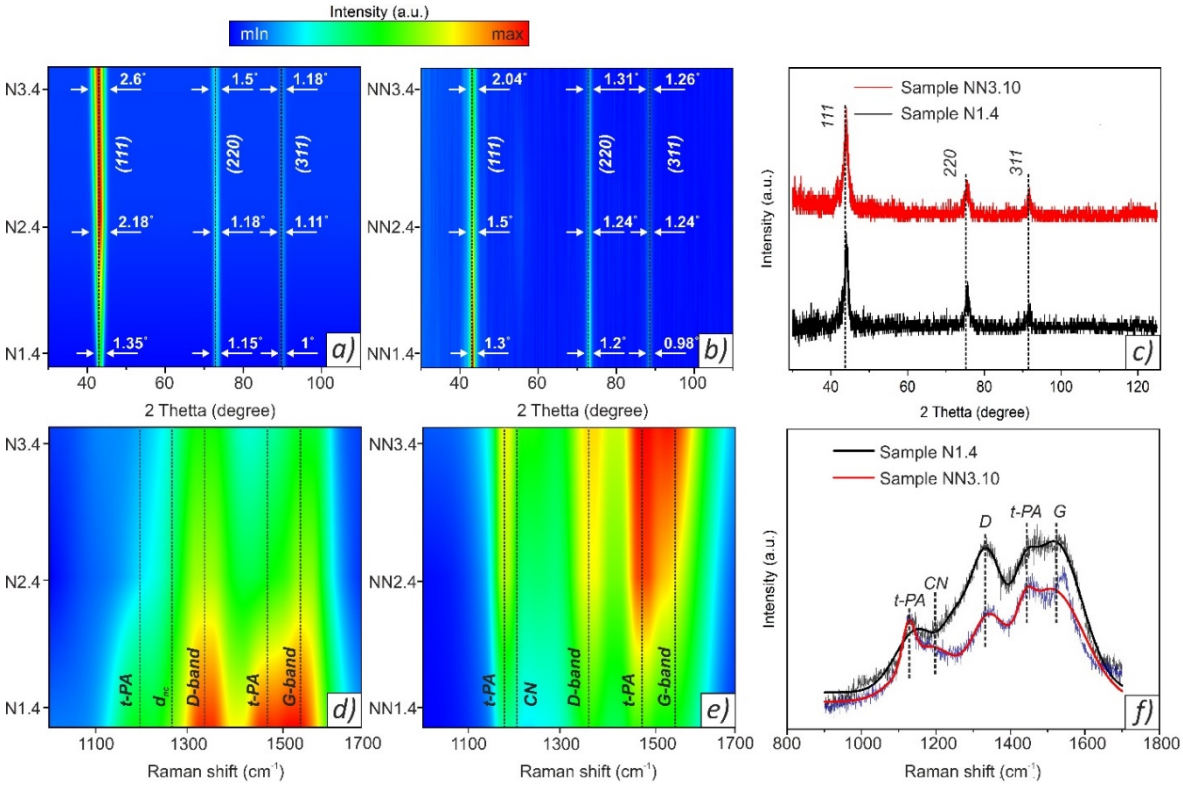

Fig.1. XRD (a-c) and Raman (a-f) spectra of deposited diamond films.

Raman spectra of deposited coatings are shown in Fig.1d and 1e. Fig.1f shows the Raman spectra with a minimum content of CH_4 and a maximum content of N_2 for comparison. As can be seen in Fig.1d, all spectra consist of five overlapping peaks which broad as methane concentration increases. Two broad peaks at 1347 and 1556 cm^{-1}, attributed to *D*- (disordered carbon) and *G*-band (graphitic domains), indicate the presence of amorphous and graphite phases of carbon occupying the grain boundaries [25]. Peaks assigned as *t-PA*, centered at 1136 and 1461 cm^{-1}, respectively, are the Raman modes of trans-polyacetylene. These peaks are considered as characteristics of ultrananocrystalline diamond (UNCD) films [26]. In addition, a peak noticed through fitting procedures and denoted as d_{nc} could be assigned as a vibrational density of state (VDOS) of small diamond crystallites or as tetrahedral amorphous carbon [26]. In this case, a characteristic dependence of the Raman spectrum on the methane concentration is observed. With an increase in the latter, the *D*- and *G*-peaks become the prevailing (derived from broadening), which indicates a decrease in the crystallinity of the synthesized coatings.

As can be seen from Fig.1e, Raman spectra of NN-series also contain *D*- and *G*-band as well as *t-PA* peaks. Moreover, in contrast to N-series, an additional peak detected at a wavelength of 1190 cm^{-1} (assign as *CN*). According to [27], this band arises due to the characteristic signature of C = N-H vibration in the diamond grain. Another difference is the absence of a peak assigned as d_{nc}, which might be due to a decrease in the intensity of the *D*-band and its significant broadening.

It is worth noting that the standard Raman spectrum deconvolution procedure did not allows to isolate the diamond peak (sp^3 carbon) at 1332.5 cm^{-1}. Nevertheless, the broadening of the *D*-peak, as well as its shift towards a lower wavenumber, indicates that this peak consists of two closely located peaks: diamond sp^3 peak at 1332.5 cm^{-1} and *D*-peak at 1347 cm^{-1}. As can be seen in Table 2 the ratio I_G/I_D decrease for both N- and NN-series due to the sp^3 carbon content change. Another important feature of the diamond films Raman spectra is a significant shift of the *G*-peak position from 1575 cm^{-1}. According to [24] induced stress (P) in diamond film could be calculated by following equation (calculated stress value are summarized in Table 2):

$$\Delta(G \text{ peak position}) = 5\ [\text{cm}^{-1}/\text{GPa}] \times P[\text{GPa}]. \quad (1)$$

Table 2. Parameters derived from Raman spectra of deposited diamond films

Samples	*D* peak FWHM, cm^{-1}	*G* peak position, cm^{-1}	I_G/I_D	Calculated induced stress, GPa
N1.10	105.6	1545	0.5	–6
N2.10	140.4	1562	0.7	–2.6
N3.10	179.1	1573	1.06	–0.4
NN1.10	117.4	1542	2.29	–6.6
NN2.10	119.2	1539	4.6	–7.2
NN3.10	122.3	1537	3.75	–7.6

The obtained data indicate that stresses dependence on the methane and nitrogen concentrations is opposite. Thus, with an increase in CH_4 concentration a decrease in stresses level from –6 to –0.4 GPa is observed. For NN-series, stress value is changed from –6.6 to –7.6 GPa.

In order to obtain more accurate data on the effect of CH_4 and N_2 gases, as well as the coating thickness on the nature and level of residual stresses in diamond coatings, the curvature method was used. According to this method, thin film residual stress can be calculated using Stoney's equation [28]:

$$\sigma_f = M_S \frac{t_S^2}{6t_f}\left(\frac{1}{R}-\frac{1}{R_0}\right)\left[1+\frac{t_f}{t_s}\left(\frac{4M_f}{M_S}-1\right)\right], \quad (2)$$

where, M_S = 193 GPa, M_f = 1220 GPa are biaxial Young's modulus of Si substrate and diamond film, t_s and t_f are substrate and film thicknesses, R and R_0 are initial and final radii of curvature of Si and diamond/Si substrates, respectively.

The calculation results are shown in Fig.2a. As can be seen, for N-series (CH_4 variation), samples N1.n and N2.n change the nature of stresses with an increase in the thickness of coatings from compressive to tensile. Similar data were previously presented in several reports [29, 30]. With a minimum coating thickness of 4 μm, the residual stress value is –0.03 GPa. Upon reaching the maximum investigated thickness of 11 μm, the calculated stress value is about 0.06 GPa. It should be noted that obtained stress values for samples N1.n and N2.n are comparable. For N3.n samples tensile nature of residual stress remains constant with an increase in the coating thickness from 4 to 11 μm. Stress value change is within 6% and amounted to 0.009 GPa.

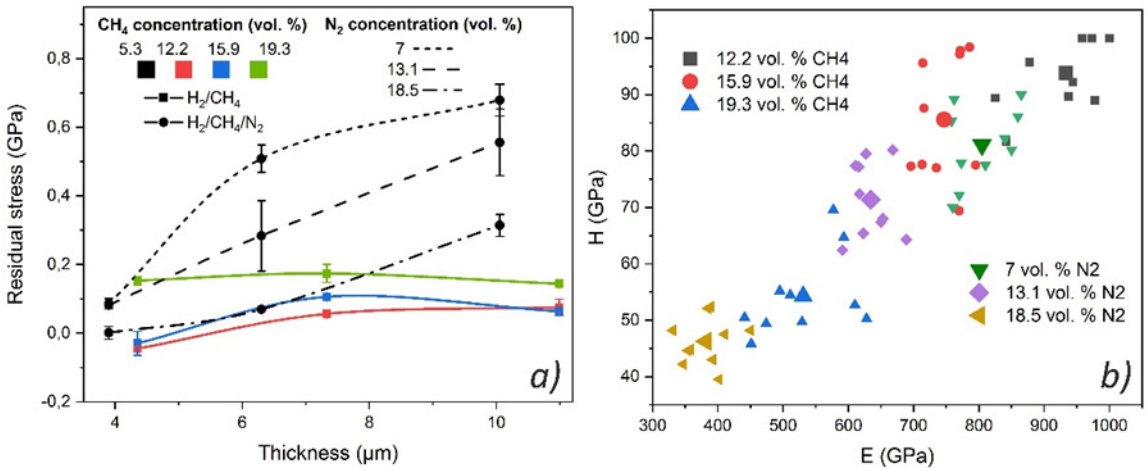

Fig.2. Residual stress (a) and *H*/*E* dependence for deposited diamond films.

For NN-series, with an increase in the nitrogen content, the magnitude of the residual stress decreases. Over the entire measurement range, the nature of the residual stresses does not change and remains tensile. The lowest stress level change is recorded for samples with the maximum nitrogen content (NN3.n series). The average value is about 0.13 GPa. Maximal stress change is observed for samples NN1.n ($\Delta\sigma_{NN1.n}$ = 0.6 GPa). Considering NN-series data, the main result is the pronounced increase in tensile stress with increase in coating thickness and its decrease with increasing in N_2 concentration. We cannot establish the origin of such dependence, but can draw a number of considerations. It is known that density of grain boundaries, i.e. crystallite size, has a significant impact on tensile component of residual stress. The smaller the crystallite size (the higher the density of grain boundaries), the greater the value of intrinsic tensile stress which in the case of diamond film cause a decrease in residual stress. Moreover, according to [31], nitrogen incorporation in diamond crystal lattice leads to an increase in its parameter and the generation of tensile stresses in the crystal. Otherwise, according to [32], coating doping leads to formation of impurities and formation of sp^2 bonded carbon at the grain boundaries which are the main source of compressive internal stress.

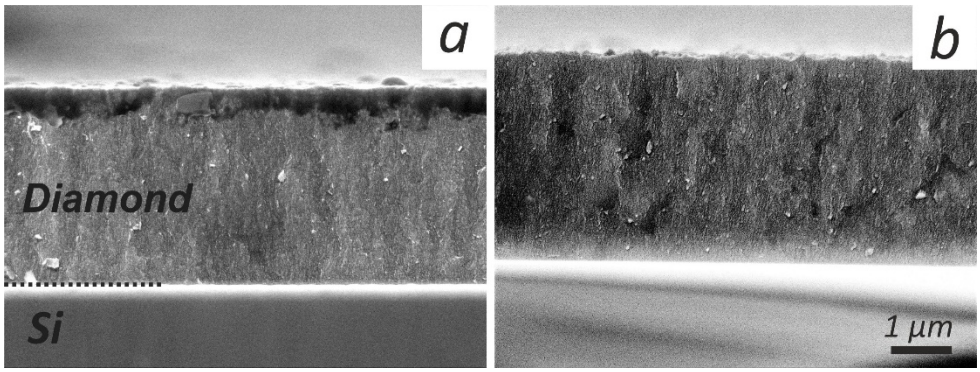

Fig.3. Cross-sectional SEM images of diamond films deposited at 12.2 vol. % CH_4 (a) and 18.5 vol. % N_2 (b).

In addition to a stresses comparative analysis, the hardness and Young's modulus values of the synthesized coatings were compared (Fig.2b). It is obvious that Young's modulus and hardness decrease as both methane and nitrogen increasing. Wherein CH_4 has a greater effect on the mechanical properties of the coating. Thus, an increase in CH_4 concentration by 7.1 vol. % leads to a decrease in coating hardness by 39.5 GPa (from 93.78 to 54.24 GPa), and the Young's modulus by

400 GPa (from 933.5 to 530.9 GPa). Increase in N_2 concentration in the gas mixture by a factor of three reduces the hardness of the coating by 34.8 GPa, and the Young's modulus by 422.2 GPa.

To clarify the effect of CH_4 and N_2 on the diamond coating structure, the obtained samples were analyzed by scanning electron microscopy (SEM). Fig.3 shows SEM micrographs of samples N1.4 and NN3.4 (extreme points for gas concentrations are shown for clarity). As can be seen in Fig.3, all films have a dense homogeneous structure without pronounced crystallinity.

The bright field TEM (BFTEM) study was performed for deeper understanding the evolution of microstructure of the films. As can be seen in Fig.4, all synthesized films have near similar structures. At these magnifications, diamond crystallites are presented as a bright sites. For each sample series (N and NN) these sites have equal size. However, N and NN-series coatings structure comparison shows that the size of the diamond crystallites of the latter is larger. This conclusion is confirmed by the selective area electron diffraction (SAED), represented as insets of Fig.4. All SEAD images show characteristic (1 1 1), (2 2 0), and (3 1 1) planes of the diamond lattice, which correspond to the randomly oriented diamond clusters. In the case of NN samples series, larger discrete diffraction spots indicate larger diamond grains or clusters.

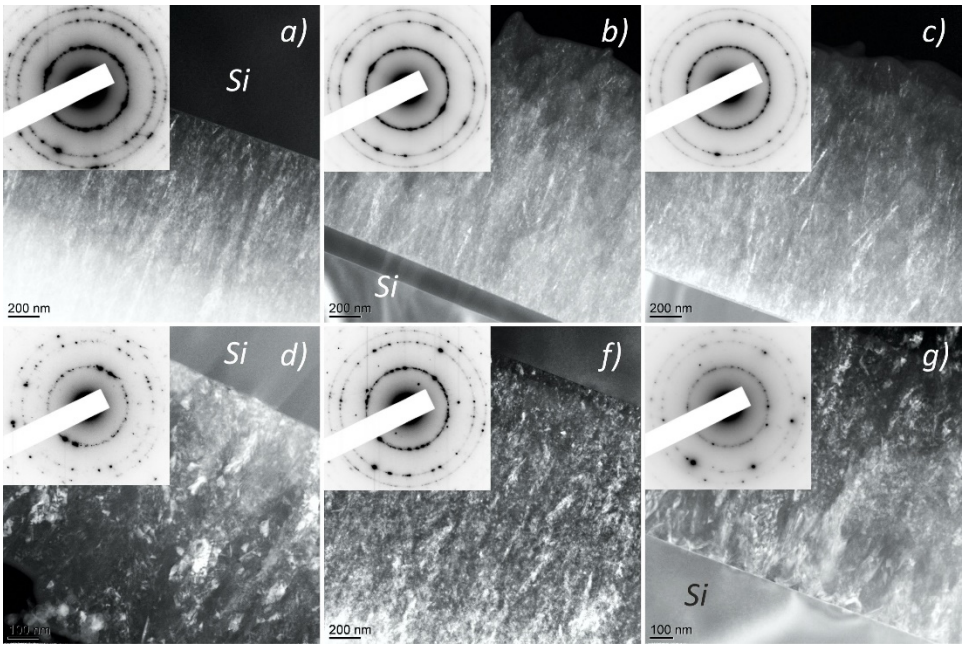

Fig.4. BFTEM and SAED images of diamond films deposited at different vol. % CH_4 (12.2 (a), 15.9 (b), 19.3 (c)) and N2 (7 (d), 13.1 (e), 18.5 (f)).

Besides, for samples synthesized in $CH_4/H_2/N_2$ gas mixture, there is an increase in the number of extra points (in the region of the outer side of the (111) ring), indicating an increase in the content of nanodiamond crystallites in the synthesized coatings. SAED patterns comparative analysis also revealed diffused ring in the center of SAEDs, indicating the existence of graphitic phase (a-C phase) in these films. Wherein nitrogen addition and further increase in its concentration leads to decrease in diffused rings intensity, which in turn indicates a decrease in a-C phase content.

A more detailed study of the synthesized coatings structures was carried out using transmission electron microscopy in the dark field mode (DFTEM). Thus, in Fig.5a and 5b one can see that diamond crystallites form agglomerations in the form of dendritic structures. The dendrites originate at the coating-substrate interface and terminate at the coating surface. The study of agglomerations in different parts of the samples showed that their size ranges from tens to hundreds of nanometers. At the same time, the minimum size of individual diamond crystallites is less than

5 nm. High resolution TEM examination of diamond films deposited at different CH_4 concentration showed the presence of randomly oriented spherical diamond particulates (~5 nm) with uniform size distribution at the coating-substrate interface (Fig.5c, zone 1).

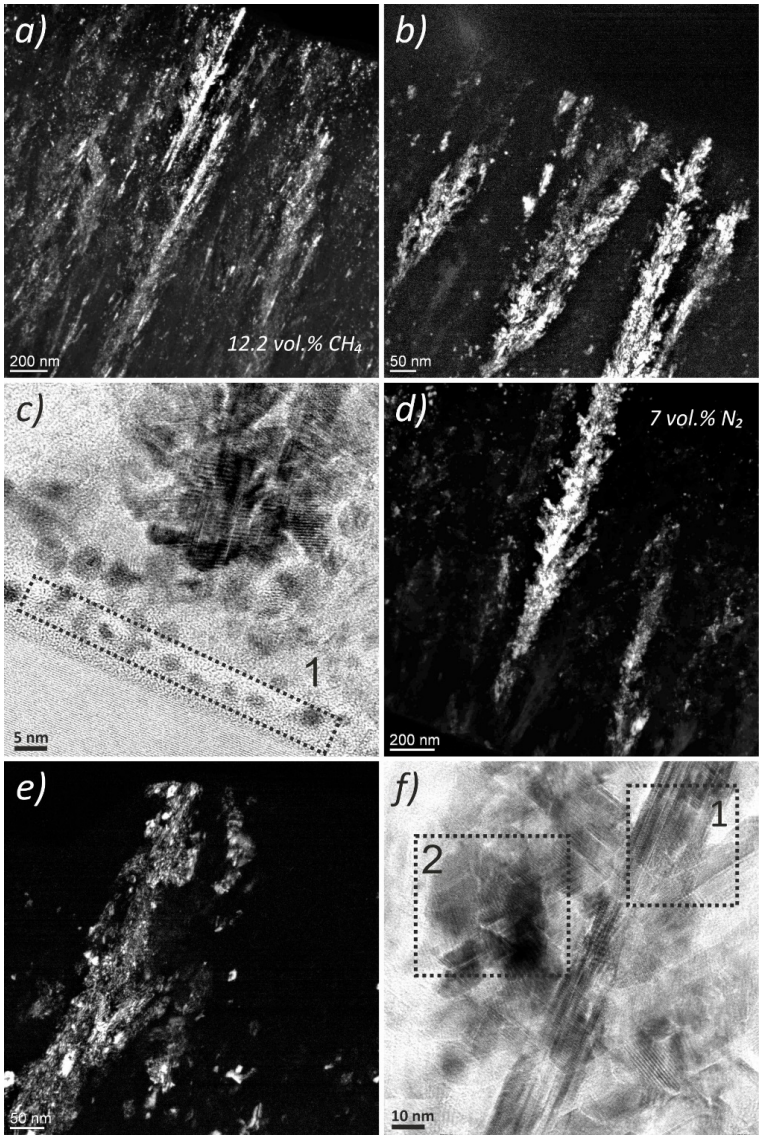

Fig. 5. DF and BFTEM images of diamond films deposited at 12.2 vol. % CH_4 (a-c) and 7 vol. % N_2 (d-f).

In the case of NN-series, no significant structure differences from the N-series were found. Films structure also presented by agglomeration in form of dendritic structures consisting of differently oriented diamond crystallites (Fig.5d–5f, zone 1), as well as spherical diamond particles (Fig.5f, zone 2). Structural feature of N-doped diamond films is absence of diamond spherical particles at the coating-substrate interface. Another feature is formation of diamond crystallites, as well as agglomerations with larger crystallite sizes (Fig.6a–6b). As can be seen in inset of Fig.6a, growth of diamond agglomerate starts from the point of self-nucleation or the introduced growth center in the form of a diamond nanoparticle.

Statement about crystallite size increasing is confirmed not only by the TEM images, but also by the surface roughness data obtained by AFM (Fig.6c and 6d). As can be seen, for both experimental series, the same dependence of the roughness on the coating thickness and CH_4 or N_2 concentration is retained. Surface roughness increases with increasing coating thickness and/or

decreasing reaction gas concentration. At the same time, the level of samples roughness N3.10 (10 µm, 19.3 vol. % CH_4) and NN1.4 (4 µm, 7 vol. % N_2) have comparable values, 16.38 and 16.6 nm, respectively. Put it different, a diamond coating with a minimum thickness and a minimum nitrogen concentration is rougher than a 10 µm thick diamond coating synthesized at the maximum methane concentration.

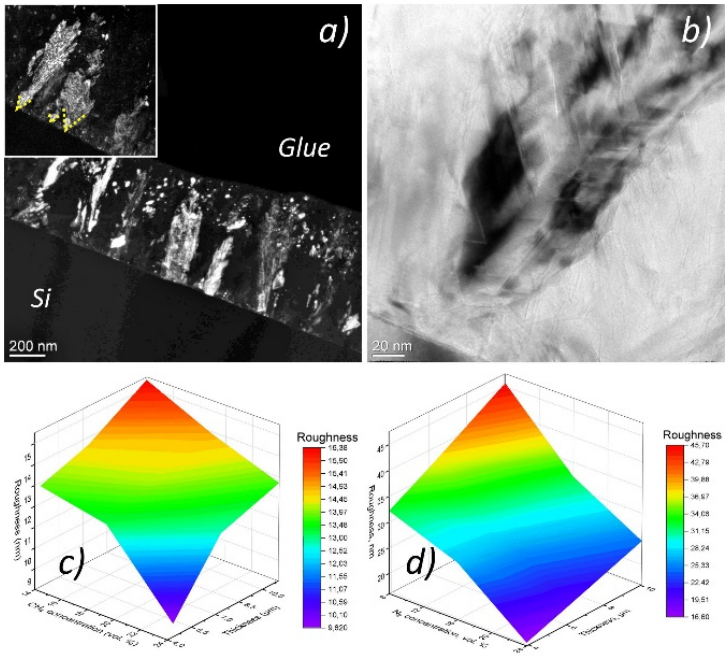

Fig. 6. DF and BFTEM images of diamond film deposited at 7 vol. % N_2 (a, b) and roughness map of N and NN-series of samples.

4. Conclusion

A comparative analysis of high CH_4 and N_2 concentration influence on structure and mechanical properties of diamond coatings was observed. Raman and XRD pattern results analysis showed (1 1 1) preferred orientation for all synthesized diamond films regardless of reaction gas type. A slight increase of crystallites size, as well as, transpolyacetelene concentration was observed for nitrogen doped coatings. A significant difference between the N- and NN-series of samples was found in the study of coatings residual stresses. Over the entire range of methane concentrations, residual stresses did not change significantly (the average value of residual stress was 0.07 GPa). With an increase in CH_4 concentration, residual stresses increased and had a tensile nature. For N_2-doped coatings, an inverse relationship was detected. With an increase in gas concentration, residual stresses decreased and their value differences became more significant. It has also been shown that hardness and Young's modulus are inversely related to the concentration of both methane and nitrogen. At the same time, methane has a greater effect on these parameters. Besides, it was found that the synthesized coatings cannot be attributed to nano- or ultrananocrystalline films, since their structure consists of a mixture of diamond dendrites and non-diamond carbon. The length of a dendrite is measured in microns, while its lateral size does not exceed 200 nm (the minimum size of detected diamond crystallites was ~5 nm).

Acknowledgement

The study was supported by the grant of the Russian Science Foundation (project no. 21-79-10004). The CVD growth equipment was created with the support by Tomsk Polytechnic University development program.

5. References

[1] Bobzin K., *Manuf. Sci. Technol.*, **18**, 2016; doi: 10.1016/j.cirpj.2016.11.004
[2] Pierson H.O., *Handb. Chem. Vap. Depos.*, **1**, 452, 1999; doi: 10.1016/b978-081551432-9.50021-8
[3] Simões R., Martins B., Santos J., Neto V., *Coatings*, **8**, 2018; doi: 10.3390/coatings8050172
[4] Pennisi C.P., *Front. Biomater.*, **1**, 70, 2014; doi: 10.2174/9781608058761114010006
[5] Nurhayati E., Juang Y., Rajkumar M., Huang C., Hu C.C., *Sep. Purif. Technol.*, **156**, 1047, 2015; doi: 10.1016/j.seppur.2015.07.022
[6] Sun Q., Wang J., Weng J., Liu F., *Vacuum.*, **137**, 155, 2017; doi: 10.1016/j.vacuum.2016.12.040
[7] Lahaye M., Manaud J.-P., Poulon-Quintin A., Hodroj A., Teulé-Gay L., *Mater. Sci.*, **5**, 519, 2018; doi: 10.3934/matersci.2018.3.519
[8] Sedov V.S., Martyanov A.K., Khomich A.A., Savin S.S., Zavedeev E.V., Ralchenko V.G., *Diam. Relat. Mater.*, **109**, 108072, 2020; doi: 10.1016/j.diamond.2020.108072
[9] Chunjiu T., José G., Neves A.J., Hugo C., Fernandes A.J.S., Lianshe F., Sérgio P., Liping G., Gil C., Carmo M.C., *Nanosci. Nanotechnol.*, **10**, 2722, 2010; doi: 10.1166/jnn.2010.1450
[10] Ullah M., Ahmed E., Welch K., Majdi S., Khalid N.R., Ahmad M., *Adv. Sci. Lett.*, **19**, 291, 2013; doi: 10.1166/asl.2013.4661
[11] Jin S., Moustakas T.D., *Appl. Phys. Lett.*, **65**, 403, 1994; doi: 10.1063/1.112315
[12] Locher R., Wild C., Herres N., Behr D., Koidl P., *Appl. Phys. Lett.,* **65**, 34, 1994; doi: 10.1063/1.113064
[13] Liu Y., Ding M., Su J., Li Y., Zhang P., Lu X., Tang W., *Diam. Relat. Mater.*, **76**, 68, 2017; doi: 10.1016/j.diamond.2017.04.009
[14] Mengui U.A., Campos R.A., Alves K.A., Antunes E.F., Hamanaka M.H.M.O., Corat E.J., Baldan M.R., *Appl. Surf. Sci.*, **334**, 222, 2015; doi: 10.1016/j.apsusc.2014.10.109
[15] Cicala G., Velardi L., Senesi G.S., Picca R.A., Cioffi N., *Appl. Surf. Sci.*, **426**, 456, 2017; doi: 10.1016/j.apsusc.2017.07.132
[16] Nemanič V., Žumer M., Kovač J., Koeck F.A.M., Nemanich R.J., *Diam. Relat. Mater.*, **50**, 151, 2014; doi: 10.1016/j.diamond.2014.10.003
[17] Roy M., Ghodbane S., Koch T., Pauschitz A., Steinmüller-Nethl D., Tomala A., Tomastik C., Franek F., *Diam. Relat. Mater.*, **20**, 573, 2011; doi: 10.1016/j.diamond.2011.02.012
[18] Wang L., Liu J., Tang T., Xie N., Sun F., *Phys. B Condens. Matter.*, **550**, 280, 2018; doi: 10.1016/j.physb.2018.09.018
[19] Sedov V., Martyanov A., Savin S., Zavedeev E., Kudryavtsev O., Bland H., Mandal S., Williams O., Ralchenko V., Konov V., *Diam. Relat. Mater.*, **114**, 108333, 2021; doi: 10.1016/j.diamond.2021.108333
[20] Sankaran K.J., Tai N.H., Lin I.N., *J. Appl. Phys.*, **117**, 2015; doi: 10.1063/1.4913258
[21] Zeng H., Moldovan N., Catausan G., *Diam. Relat. Mater.*, **91**, 165, 2019; doi: 10.1016/j.diamond.2018.11.016
[22] Song X., Wang H., Wang X., Sun F., *Diam. Relat. Mater.*, **117**, 108487, 2021; doi: 10.1016/j.diamond.2021.108487
[23] Ficek M., Sankaran K.J., Ryl J., Bogdanowicz R., Lin I.N., Haenen K., Darowicki K., *Appl. Phys. Lett.*, **108**, 2, 2016; doi: 10.1063/1.4953779
[24] Heiman A., Lakin E., Zolotoyabko E., Hoffman A., *Diam. Relat. Mater.*, **11**, 601, 2002; doi: 10.1016/S0925-9635(01)00631-8
[25] Titovich K.A., Kumar N., Vyacheslavovich S.A., Ivanovich K.V., Rani R., Panda K., Lin I.-N., *Sci. Rep.*, **8**, 1, 2018; doi: 10.1038/s41598-017-18425-4

[26] Memmel N., Kaindl R., Bertel E., Klauser F., Steinmüller-Nethl D., *Chem. Vap. Depos.*, **16**, 127, 2010; doi: 10.1002/cvde.200906827
[27] Cherf S., Chandran M., Michaelson S., Elfimchev S., Akhvlediani R., Hoffman A., *Thin Solid Films.*, **638**, 264, 2017; doi: 10.1016/j.tsf.2017.07.060
[28] Kim J.G., Yu J., Cho D.H., Baik Y.J., *Diam. Relat. Mater.*, **9**, 61, 2000; doi: 10.1016/S0925-9635(99)00229-0
[29] Gaydaychuk A., Linnik S., *Int. J. Refract. Met. Hard Mater.*, **85**, 2019; doi: 10.1016/j.ijrmhm.2019.105057
[30] Kim J.G., Yu J., *Jpn. J. Appl. Phys.*, **37**, L890, 1998; doi: 10.1143/JJAP.37.L890
[31] Gusakov G.A., Samtsov M.P., Voropay E.S., *J. Appl. Spectrosc.*, **85**, 279, 2018; doi: 10.1007/s10812-018-0645-1
[32] Ding M.Q., *Res. Dev. Mater. Sci.*, **11**, 1175, 2019; doi: 10.31031/rdms.2019.11.000762